



HAL
open science

Experimental study of oxidation in oxygen, nitrogen and steam mixtures at 850°C of pre-oxidized Zircaloy-4

Mathilde Gestin, Michel Mermoux, Olivia Coindreau, Christian Duriez,
Michèle Pijolat, Véronique Peres, Loïc Favergeon

► To cite this version:

Mathilde Gestin, Michel Mermoux, Olivia Coindreau, Christian Duriez, Michèle Pijolat, et al.. Experimental study of oxidation in oxygen, nitrogen and steam mixtures at 850°C of pre-oxidized Zircaloy-4. Journal of Nuclear Materials, 2019, 519, pp.302 à 314. 10.1016/j.jnucmat.2019.03.020 . hal-02152759

HAL Id: hal-02152759

<https://hal.science/hal-02152759>

Submitted on 17 Oct 2019

HAL is a multi-disciplinary open access archive for the deposit and dissemination of scientific research documents, whether they are published or not. The documents may come from teaching and research institutions in France or abroad, or from public or private research centers.

L'archive ouverte pluridisciplinaire **HAL**, est destinée au dépôt et à la diffusion de documents scientifiques de niveau recherche, publiés ou non, émanant des établissements d'enseignement et de recherche français ou étrangers, des laboratoires publics ou privés.

Experimental study of oxidation in oxygen, nitrogen and steam mixtures at 850°C of pre-oxidized Zircaloy-4

M. Gestin^{a,b}, M. Mermoux^c, O. Coindreau^{a,*}, C. Duriez^a, M. Pijolat^b, V. Peres^b, L. Favergeon^b

a Institut de Radioprotection et de Sûreté Nucléaire, PSN-RES, Cadarache BP 3, 13 115 St Paul-Lez-Durance Cedex, France

b Mines Saint-Etienne, Univ Lyon, CNRS, UMR 5307 LGF, Centre SPIN, F-42023, Saint-Etienne, France

c Université Grenoble Alpes, LEPMI, UMR 5279 CNRS, 38402, Saint-Martin d'Hères Cedex, France

* Corresponding author : e-mail address: olivia.coindreau@irsn.fr (O. Coindreau).

abstract

Since the Fukushima Daiichi accident, increased attention is paid to the vulnerability of Spent Fuel Pools (SFPs). In case of an accidental dewatering of the fuel assemblies, the fuel cladding would be exposed to an air-steam atmosphere and its oxidation is a key phenomenon since it drives the fuel assembly heat-up and degradation. In this study, we have investigated the corrosion kinetics of pre-oxidized and as-received Zircaloy-4 (Zy-4) plate samples at 850°C. The low temperature pre-oxidation aims at simulating the corrosion scale that grows during the in-reactor use of the fuel. High temperature oxidation tests were carried out under mixed oxygen-steam-nitrogen atmospheres. In the different atmospheres investigated, a rather protective effect of the pre-oxide scale regarding subsequent high temperature oxidation has been observed, for limited time periods however. Post-test examinations of the samples demonstrated that the loss of the protection was associated to the spalling of the pre-oxide scale that initiated at sample edges, where the pre-oxide scale was cracked. For the steam partial pressure range investigated in this study (0-8 vol%), there was no noticeable effect of the steam partial pressure on the oxidation rate. Nevertheless, samples hydrogen pick-up were strongly correlated to steam partial pressures. Moreover, ¹⁸O isotopic labelling experiments suggested that the contribution of O₂ and H₂O to the oxidation process corresponds to their respective concentration in the gas phase.

1. Introduction

During a loss of cooling or loss of coolant accident in a Spent Fuel Pool (SFP), the failure of safety systems could lead to the dewatering of the fuel assemblies [1]. The uncovering of fuel rods would occur faster if a fuel assembly is being handled when the cooling and/or coolant is lost. As a consequence, the fuel assemblies would be exposed to an air-steam atmosphere. In these conditions, the cladding temperature increases owing to the fuel residual decay heat and when the

temperature reaches about 600°C, oxidation becomes significant. The oxidation of the uncovered part of the fuel assemblies is one of the determining phenomena for the accident progression [2]. On the one hand, the oxidation drives the fuel heat-up, due to the important heat of the Zy-4 oxidation reaction. On the other hand, the oxidation in air-containing environments leads to the degradation of the Zy-4 cladding with the formation of a porous oxide layer. Unlike what is expected for reactor Loss Of Coolant Accident (LOCA) scenarios (at least in the early phase, before vessel failure), air is present in the atmosphere. This is an aggravating factor because of the catalytic role of nitrogen on the oxidation mechanism, i.e. complex, simultaneous and fast oxidation and nitriding processes. As a matter of fact, high temperature (HT) oxidation of pure Zr or Zr-based alloys is by far much faster in nitrogen-containing environments (oxygen and/or steam), than in nitrogen-free atmospheres, as early shown by the works of Hayes and Roberson [3], Evans et al. [4], Leistikow and Berg [5]. Since then, other studies have confirmed this trend [6-9]. In each of these studies, nitrogen is observed to strongly affect the Zr oxidation mechanism when present in the reacting gas.

From a thermodynamic point of view, the Gibbs free energy of the $\text{Zr} + \text{O}_2 \rightarrow \text{ZrO}_2$ reaction is -888 kJ/mol at 850°C, nearly twice that of the $\text{Zr} + 2\text{H}_2\text{O} \rightarrow \text{ZrO}_2 + 2\text{H}_2$ reaction (-516 kJ/mol at 850°C). Both steam and oxygen can oxidize zirconium, but oxidation by oxygen is the most thermodynamically favorable and also the most exothermic process. Moreover, zirconia formation is thermodynamically much more favorable than zirconium nitride formation, given that the Gibbs free energy of the $\text{Zr} + 0.5 \text{N}_2 \rightarrow \text{ZrN}$ reaction is equal to -260 kJ/mol. However, ZrN was systematically observed close to the metal/oxide interface when bare Zy-4 was oxidized in air at a temperature higher than 800°C [7,8,10]. It was consequently proposed that the formation of ZrN and its further re-oxidation is responsible for the significant cladding material degradation [4,7,8]. The effect of nitrogen is particularly strong in the 600-1000°C temperature range since it leads to early kinetic transition and subsequent accelerated oxidation. A kinetic model, based on surface nucleation and growth of regions attacked by nitrogen [11], enables to account for the fast oxidation of bare Zy-4 in dry air at 850°C. In steam-air atmospheres, less data are available. Steinbrück et al. [8] and Negyesi et al. [12] showed that the weight gain of Zy-4 fuel cladding exposed to an air-steam atmosphere strongly depends on the air fraction in steam. Moreover, Steinbrück et al. [8] analysed the reaction gas products with Mass Spectrometry during the oxidation tests. At 1000°C, hydrogen was measured only during the test in pure steam. Increasing the oxidation temperature up to 1500°C, hydrogen was measured in all tests conducted with less than 50 vol% air in the mixture. They concluded that in these oxidation conditions, oxygen is first consumed completely, initially at the beginning of the HT oxidation, and then oxidation by steam can take place.

To study the oxidation of fuel rods stored in a SFP, the presence of the corrosion oxide scale formed during in-service operation in reactor has to be taken into account. The effect of a very thin pre-oxide layer ($\approx 1 \mu\text{m}$) on subsequent high temperature steam oxidation of Zy-4 was studied by Kawasaki et al. [13]. More recently, the effect of a pre-oxide scale on subsequent HT oxidation of zirconium alloys was investigated on Zy-4 cladding materials, under steam [14-17] or under oxygen-nitrogen atmospheres [18]. Results of air oxidation in the 850-1000°C temperature range of pre-oxidized cladding tubes [18] indicate that a pre-oxide layer of approximately 30 μm acts, for a limited time period (a few hours at maximum), as a protective layer against further HT oxidation. Examination of the open literature shows that rather limited works on the degradation of pre-oxidized Zy-4 exposed to air-steam is available. Therefore, the aim of this study is to bring new data

concerning the oxidation rate of pre-oxidized Zy-4 samples exposed to nitrogen-containing atmospheres.

For such a purpose, Zy-4 plate samples have been first oxidized at low temperature to obtain a so-called pre-oxide layer of about 30 μm in thickness. The aim was to form, as far as possible, an oxide scale representative of the external corrosion scale of spent fuel rods. In this study, the irradiation effects were not taken into account. After pre-oxidation, a large amount of isothermal oxidation tests in mixed nitrogen-steam and in mixed steam-air atmospheres (with various steam fractions ranging from 0 up to 8 vol% that is 0-80 hPa) were carried out at 850°C. A 850°C temperature was chosen since it enables the observation of the nitrogen-“catalyzed” regime over a period of time long enough for minimizing temperature and partial pressure gradients in the reacting system. Helium was used to dilute the reacting gas in order to change the partial pressure of only one reacting gas at one time without changing the partial pressures of the other gases. The oxidation process has been analysed in light of metallographic observations and hydrogen pick-up measurements. Moreover, tests using labelled $^{18}\text{O}_2$ and H_2^{16}O have been carried out. The ^{18}O concentration in the oxide scale was determined by Raman Spectrometry and is a first attempt to point out the proportion of oxygen/steam reacting to form the HT oxide.

2. Experimental

2.1. Samples

The specimens used in this study were cut from low tin Stress-Relieved Annealed (SRA) Zircaloy-4 sheet provided by Framatome to 15 mm \times 10 mm plates, 475 μm in thickness. The 15 mm length is oriented along the rolling direction of the sheet. The alloy composition is given in Table 1.

Alloy	Sn (wt.%)	Fe (wt.%)	O (wt.%)	Cr (wt.%)	C (ppm)	Nb (ppm)	H (ppm)
Zy-4	1.32-1.35	0.21	0.123-0.129	0.11	125-140	< 40	< 3

Table 1. Composition of the Zy-4 alloy.

Some of the samples were used in the as-received state whereas the others were pre-oxidized in a mixed oxygen-steam (15 vol%) atmosphere. Steam was added to the oxidizing atmosphere to promote hydrogen incorporation in the metal during the low-temperature (LT) oxidation, targeted to be similar to the one observed under PWR irradiation for Zircaloy-4. Oxidation took place at atmospheric pressure in a horizontal resistive furnace at a temperature of 425°C. These pre-oxidation conditions were chosen to keep reasonable pre-oxidation time while avoiding recrystallization of the alloy. To control the oxide growth rate, selected specimens were periodically extracted from the furnace and weighted with a 0.1 mg accuracy (each 20-50 days). A roughly linear growth rate of approximately 0.12 μm per day was deduced from the weight gains. Thus, it took about 250 days to reach the targeted thickness of approximately 30 μm . Pre-oxide thicknesses were systematically calculated from weight gains assuming a 97% theoretical density of the monoclinic zirconia and neglecting the mass contributions of oxygen dissolution and hydrogen pick-up in the metal. Mean sample thicknesses were in the 26.6-32.7 μm range for the specimens used in this study. A metallographic observation of one of these samples is shown in Fig. 1. Hydrogen contents after pre-oxidation ($[\text{H}]_{\text{PO}}$) were determined by the fusion technique in some samples. The concentrations were in the 270-300 ppm range. Detailed characterization of the pre-oxide scales obtained with this protocol had been performed using XRD, Raman spectroscopy and SEM/FEG

observations. Results were presented in previous papers, and the representativeness of the obtained scale regarding in-PWR corrosion was discussed as well [19,20].

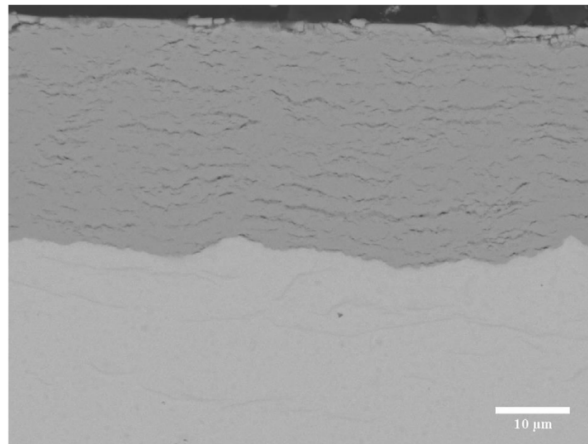


Fig. 1. SEM micrograph of the pre-oxide scale formed on Zircaloy-4 at 425°C in oxygen and 15 vol% steam.

2.2. Thermogravimetric analysis (TGA)

High temperature oxidation experiments, as well as ^{18}O exposure tests, were systematically performed at 850°C. Corrosion kinetics in $\text{O}_2\text{-N}_2$ (in air proportion)-He- H_2O flowing mixtures were followed using a symmetrical microbalance (SETARAM-TAG24). The use of a double furnace symmetrical thermobalance allowed a direct compensation of Archimedes' buoyancy and thermohydraulic effects. Samples were placed in a platinum wire basket and suspended in the furnace via a platinum hook. Platinum was chosen to limit interaction between the sample and the basket as no eutectoid reaction was observed for the temperature range investigated. The use of such a wire basket was needed to retrieve the pre-oxide fragments that can be lost during the high-temperature oxidation. To check that the wire basket did not limit the access of the oxidizing atmosphere to the sample surface, we compared the mass gain rate of a pre-oxidized sample placed in a wire basket with that of a pre-oxidized sample directly hanged to a platinum hook. The measurements were similar, attesting that the wire basket did not limit gas supply. A specific alumina plate sample was placed in the reference furnace in order to minimize baseline drifts during experiments.

Oxygen, nitrogen, steam and helium were injected from the bottom and flowed up into the furnace chambers. Steam was produced by evaporation of a controlled water flow in a heated coil and mixed with the other gases. Gas lines between the steam generator and the thermobalance were heated above 80°C to prevent steam condensation. The partial pressures could be adjusted controlling the flow rate of the different species, keeping constant a 3 NL/h per furnace total flow rate. The conditions for all experiments are given in Table 2. Flow rates were sufficient to avoid insufficient reactive gas supply since the oxygen mass flow rate was one order of magnitude higher than the maximum measured mass gain rate. The steam partial pressure range investigated in this study was limited by the maximum steam partial pressure allowed in the thermobalance. Helium dilution was adopted to keep constant O_2 and N_2 partial pressures while H_2O was added to the gas phase. This allowed an easier comparison of the different kinetic data. The gas mixture was injected at room temperature and a heating ramp of $30^\circ\text{C}\cdot\text{min}^{-1}$ was imposed up to 850°C. Indeed a previous study [9] has shown that the introduction of the reactive mixture once the isothermal condition is reached

after the temperature ramp under inert gas leads to non reproducible mass change curves. At the end of the isothermal oxidation tests, sample cooling was also performed in the reactive atmosphere with a cooling rate of approximately $50^{\circ}\text{C}\cdot\text{min}^{-1}$. A quadrupole mass spectrometer (Hiden Analytical) was connected to the outlet of the furnace through a capillary. This allowed a continuous analysis of all gaseous species, including hydrogen and steam. The measure was qualitative as no calibration of the mass spectrometer had been done. If applicable, the hydrogen release rate was tentatively used to follow the variations of the reaction kinetics.

Flow rates (NL/h)					Partial pressure (hPa)		
He	O ₂	N ₂	H ₂ O	Total	P _{O₂}	P _{N₂}	P _{H₂O}
5.52	0.48	0	0	6	80	0	0
5.7	0	0	0.3	6	0	0	50
5.222	0.48	0	0.3	6	80	0	50
3.78	0	1.92	0.3	6	0	320	50
3.6	0.48	1.92	0	6	80	320	0
3.42	0.48	1.92	0.18	6	80	320	30
3.3	0.48	1.92	0.3	6	80	320	50
3.12	0.48	1.92	0.48	6	80	320	80
He	¹⁸ O ₂	N ₂	H ₂ O	Total	P _{O₂}	P _{N₂}	P _{H₂O}
5.66	0.06	0.24	0.0375	6	10	40	6.25

Table 2. Flow rates and corresponding partial pressures used for high temperature TGA oxidation tests with plates in diluted air-steam atmospheres. The partial pressures are calculated on the basis of a 1000 hPa total pressure and the flow rates are given at standard temperature and pressure (273.15 K, 1 bar).

A similar protocol was followed for ¹⁸O exposure tests, using a mixture of ¹⁸O₂, H₂¹⁶O and N₂. To limit ¹⁸O consumption, the oxygen flow rate used for ¹⁸O tests was divided by a factor of 8 (0.06 L/h instead of 0.48 L/h). The steam mass flow rate was also decreased to keep the same P_{H₂O}/P_{O₂} ratio as in the reference conditions (80 hPa O₂ - 320 hPa N₂ - 50 hPa H₂O). For the analysis of ¹⁸O exposure tests, we used the ¹⁸O/¹⁶O ratio that corresponds to the number of ¹⁸O atoms divided by the number of ¹⁶O atoms, namely 2P_{O₂}/P_{H₂O} (which is 3.2). We also used the ¹⁸O/O ratio, defined as the number of ¹⁸O atoms divided by the total number of O atoms, namely 2P_{O₂}/(2P_{O₂} + P_{H₂O}) (which is 0.76).

2.3. Metallographic examinations and hydrogen pick-up

After oxidation tests, the specimens were cut along their 15 mm length (along the rolling direction of the Zircaloy-4 sheet), close to the center axis of the plate, avoiding the hole however. One part was cold embedded in epoxy resin and polished with a MECAPOL P320 PRESI device for metallographic examinations, using optical microscopy (Olympus PMG3 and Keyence VHX-5000) and/or scanning electron microscopy (SEM) (Zeiss SUPRA 55 VP). The second part was used to determine the hydrogen pick-up by the fusion technique. Before the measurement, the oxide scales were removed by sand blasting, both for pre-oxidized and high-temperature oxidized specimens. As most of the incorporated hydrogen is retained in the metal, the oxide scales were removed by sand-blasting before the measurement, to get rid of the zirconia contribution to the sample mass. A 100 μm grain-size corundum media was used. Part of the α-Zr(O) layer was also ablated during the process. However, this is believed not to affect strongly the hydrogen measurement results because the oxygen enriched α-Zr phase is known to be hydrogen-depleted [21]. For each specimen, 6 different measurements were done, and an average value determined.

2.4. ¹⁸O concentration determination using Raman spectroscopy

Raman imaging measurements were performed using a RM1000 Renishaw spectrometer. This spectrometer gave a good compromise between spectral resolution, spatial resolution and luminosity. It was equipped with an air-cooled CCD detector and a microscope. The excitation wavelength was the 514 nm line of an Ar⁺ ion laser. The power at the specimen was a few mW. Spectra were acquired using a 50x (numerical aperture or NA = 0.75) objective. Cross sections were examined. The sizes of the examined areas were chosen to get representative maps for each specimen. They were examined with a point spacing of 1 μm or less, if necessary. The whole procedure to extract ¹⁸O profiles or maps from Raman mapping experiments has already been detailed in [19,22]. Briefly, the particular monoclinic ZrO₂ line, peaking at about 475 cm⁻¹ when no ¹⁸O is incorporated in the m-ZrO₂ oxygen sub-lattice, intense and isolated from the other lines, was used to extract the ¹⁸O content in zirconia scales. As shown in [22], the line downshift versus the ¹⁸O content was strong, estimated and measured to about 0.27 cm⁻¹ / ¹⁸O at.%. As shown by [22], stress and alloying effects may also modify the position of this particular Raman line. However, these effects are small compared to the main isotopic effects. Actually, different measurements conducted on pre-oxide scales grown in pure ¹⁶O environments have shown that the stress-induced or even alloying-shift are rather small and do not exceed 1.5 cm⁻¹. As discussed in [19], the overall uncertainty on these measurements was about 5%, and was all the more important that the measured ¹⁸O contents were low. This is why we systematically used high ¹⁸O content, for which the expected line shifts are by far higher than 1.5 cm⁻¹. In such cases, it has been shown that Raman and SIMS images compare well [19,23], and that stress effects can be neglected.

3. Results

3.1. Effect of the pre-oxide scale

The mass change and kinetic rate of as-received and pre-oxidized samples are displayed in Fig. 2 for HT oxidation at 850°C under 80 hPa O₂-320 hPa N₂-50 hPa H₂O. For both samples, there is an increase of the mass gain rate during the heat-up phase, attesting that oxidation starts before isothermal conditions are reached. The mass gain of the pre-oxidized sample during the heat-up phase is very limited compared to that of the as-received sample. During this phase, it is expected that oxygen first migrates from the pre-oxide scale into the metallic substrate, leading to chemical reduction of the zirconia. Nevertheless, for the oxidizing conditions and heat-up rate used in this study, it was demonstrated that this phenomenon has a negligible impact on the mass gain [19]. When isothermal conditions are reached, the mass gain rate of the as-received sample decreases, which corresponds to the “pre-transition” stage during which the oxide growth kinetics is known to be controlled by oxygen vacancy diffusion through a growing dense zirconia layer. After approximately 3000 s at 850°C, the mass gain rate reaches a minimum value which corresponds to a “kinetic transition”, associated to the formation of first cracks in the dense zirconia layer. During the “post-transition” stage, cracks in the oxide layer spread over the surface of the sample allowing gas phase diffusion into the cracked oxide scale [9] with a catalytic effect of nitrogen [11]. The behavior of the pre-oxidized sample is completely different since the mass gain rate always increases. During the first 5000 s at 850°C, the oxidation rate of the pre-oxidized sample is lower than that of the as-received sample, demonstrating the protective character of the pre-oxide layer at the beginning of the HT oxidation process. After 5000 s at 850°C, the oxidation rate of the pre-oxidized sample is the same or even higher than that of the as-received sample. It shows that the protective effect of the pre-oxide scale has limited time duration.

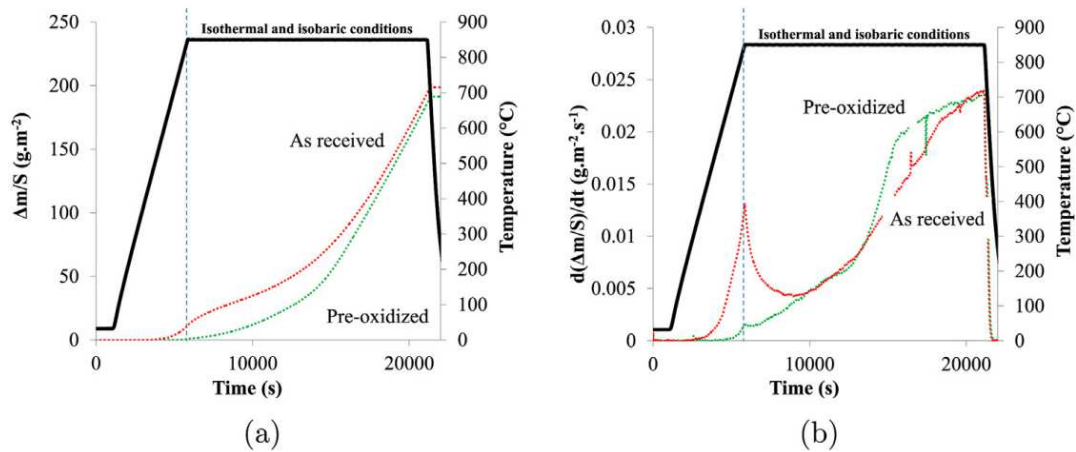


Fig. 2. (a) Mass gain and (b) mass gain rate as a function of time of as-received (red line) and pre-oxidized (green line) Zy-4 plate samples oxidized at 850°C in 80 hPa O₂ - 320 hPa N₂ -50 hPa H₂O.

Optical and SEM images show that the thickness of the HT oxide layer is greater near the edges of the sample (see Fig. 3b). In addition, they show the presence of large cracks at the edges of the samples, which penetrate through the whole oxide thickness up to the metal (see Fig. 3a). These cracks are initially present on all pre-oxidized samples, and are formed during the cooling from 425°C down to room temperature or during the low temperature oxidation process. These observations show that the oxidation front progresses laterally in the sample, under the pre-oxide layer. This is a strong indication that any crack or defect in the pre-oxide scale may be an initiating point for the HT oxidation. Moreover, above the HT oxide scale, the pre-oxide scale is no more adherent. The lateral progression of the HT oxide and the associated spalling of the pre-oxide layer allow to explain the loss of the pre-oxide scale protectiveness. This occurs rapidly for the samples used in this study since the length of the cracks (which is approximately the length of the edges) relative to the surface area is high ($\approx 0.33 \text{ mm}^{-1}$). Far away from the edges, where the pre-oxide scale is still adherent (left hand side of Fig. 3b), it is not possible to distinguish by optical microscopy the HT scale below the pre-oxide scale. It means that if present, the HT scale is here very thin and that its contribution to the mass gain is low. Nevertheless, ZrN particles can be seen at the metal/oxide interface (see Fig. 8b). These observations are in agreement with the conclusions of [19] that reported that nitrogen diffuses through a pre-oxide layer much faster than oxygen and accumulates close to the metal/oxide interface.

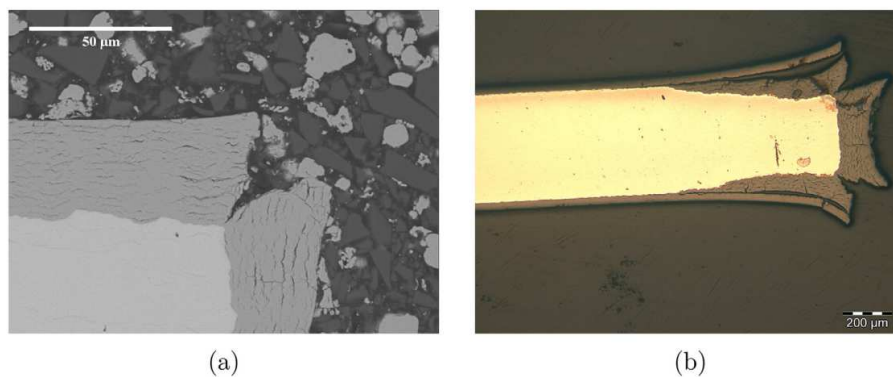


Fig. 3. (a) SEM micrograph of the edge of a Zy-4 plate sample pre-oxidized at 425°C; (b) Optical image of a pre-oxidized Zy-4 plate sample oxidized at 850°C under 80 hPa O₂ - 320 hPa N₂ -50 hPa H₂O during 76 min (4560 s).

3.2. Effect of the gas phase composition on the oxidation rate

The mass gain rates of pre-oxidized samples exposed to nitrogen-containing and nitrogen-free atmospheres are displayed in Fig. 4. The mass gain rate of a pre-oxidized sample exposed to a mixed oxygen-nitrogen atmosphere is by far greater than that of a pre-oxidized sample exposed to oxygen only (Fig. 4a). Under pure oxygen, the mass gain rate starts to decrease when isothermal conditions are reached. After 5000 s at 850°C, it remains constant and after 8000 s, it slightly increases. This indicates that the pre-oxide scale is not perfectly protective, due to the presence of cracks at the edges of the pre-oxide scale. But the mass gain rate remains low ($0.002 \text{ g m}^{-2} \text{ s}^{-1}$). When the pre-oxidized sample is exposed to a mixed oxygen - nitrogen atmosphere, the mass gain rate does not stop increasing. After 15000 s at 850°C, the mass gain rate is $0.025 \text{ g m}^{-2} \text{ s}^{-1}$, that is more than an order of magnitude higher than that measured under oxygen. Similarly, the mass gain rates of pre-oxidized samples exposed to steam-nitrogen or to oxygen-steam-nitrogen are higher than that measured under steam (see Fig. 4b) or under oxygen-steam (see Fig. 4c). The kinetic rates are much higher when nitrogen is present in the gas phase, as already observed for bare Zy-4 [8].

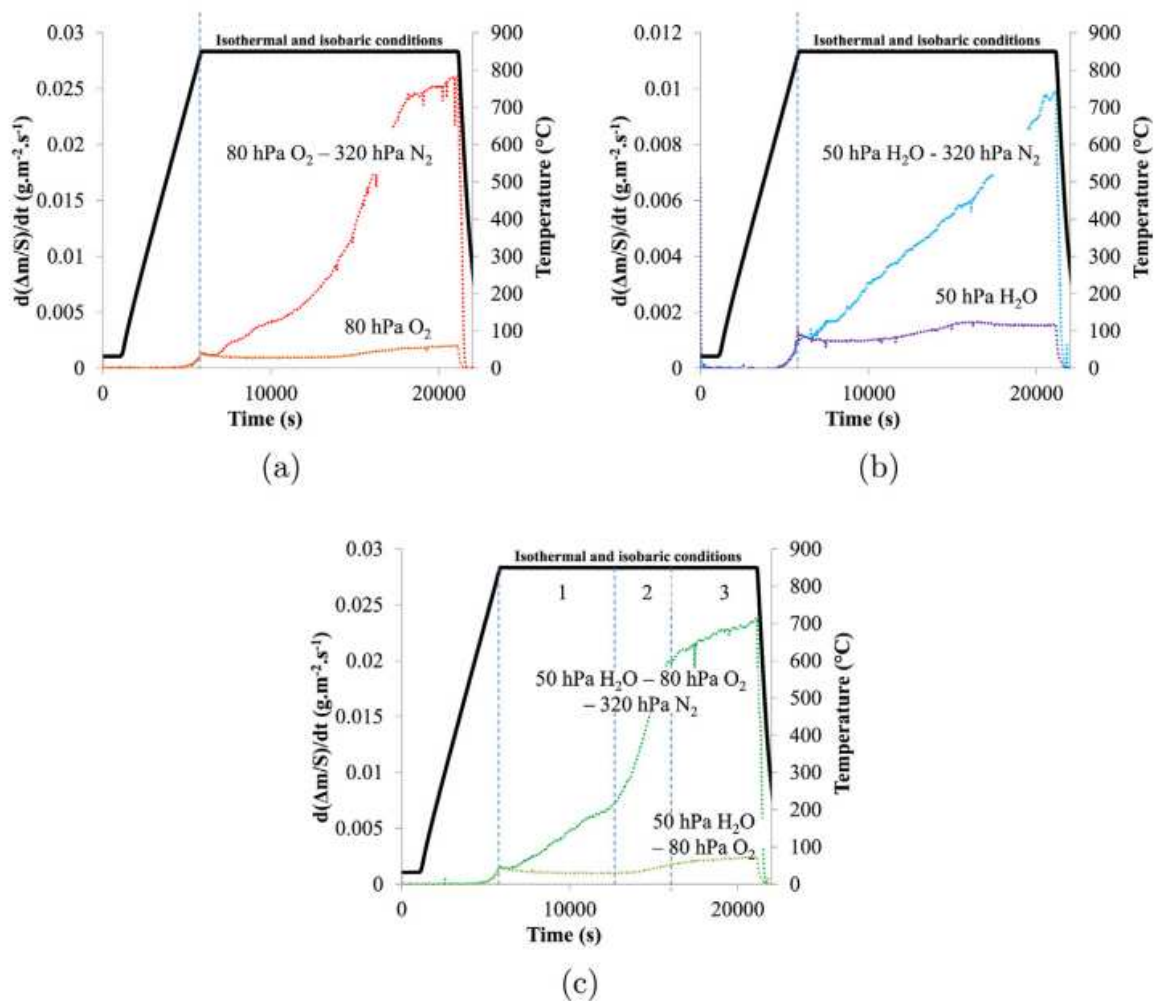


Fig. 4. Mass gain rate as a function of time of a pre-oxidized Zy-4 plate sample oxidized at 850°C in (a) 80 hPa O₂ -320 hPa N₂ (red line) and in 80 hPa O₂ (orange line); (b) 320 hPa N₂ -50 hPa H₂O (blue line) and in 50 hPa H₂O (purple line); (c) 80 hPa O₂ -320 hPa N₂ -50 hPa H₂O (dark green line) and in 80 hPa O₂ -50 hPa H₂O (green line).

To understand the effect of steam when added to air on the oxidation kinetics, a range of steam partial pressures was further considered and varied in the 0-80 hPa partial pressure range in the gas phase, while keeping constant oxygen and nitrogen partial pressures by means of helium dilution. The results obtained are displayed in Fig. 5. For the pressure range investigated here, the effect of the steam partial pressure is very weak: the mass gain rates measured in the different atmospheres are very similar with a little increase of the mass gain rate when steam is added to air.

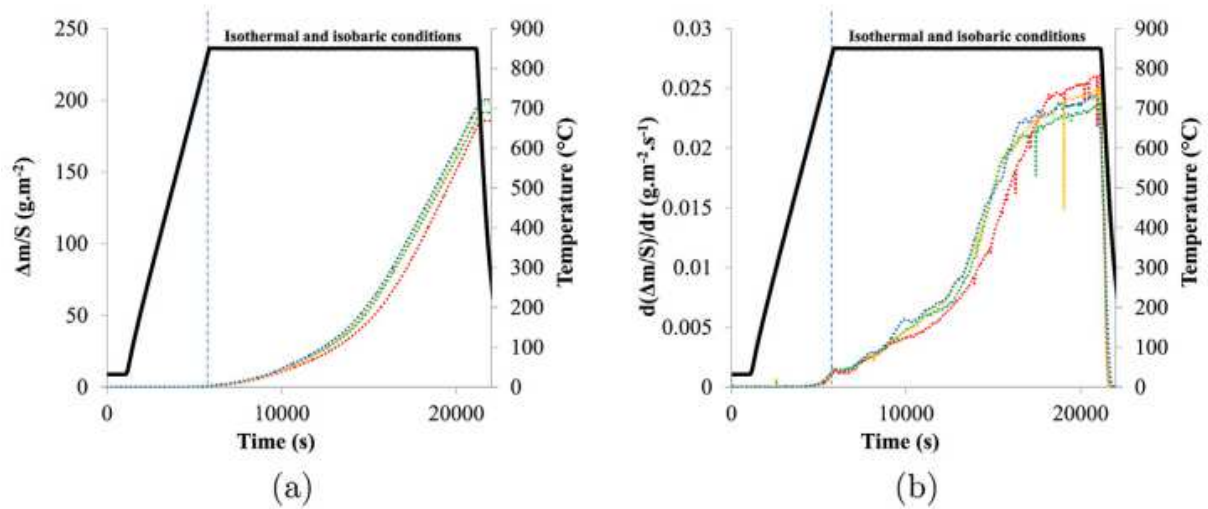


Fig. 5. (a) Mass gain and (b) mass gain rate as a function of time of a pre-oxidized Zy-4 plate sample oxidized at 850°C in 80 hPa O₂ - 320 hPa N₂ - x hPa H₂O (x=0 hPa red; x=30 hPa yellow; x=50 hPa green; x=80 hPa blue).

Cross sectional optical images obtained after the HT oxidation tests on pre-oxidized Zy-4 samples are displayed in Fig. 6. On the left side, the samples were oxidized in nitrogen-containing atmosphere whereas on the right side they were oxidized in nitrogen-free atmospheres.

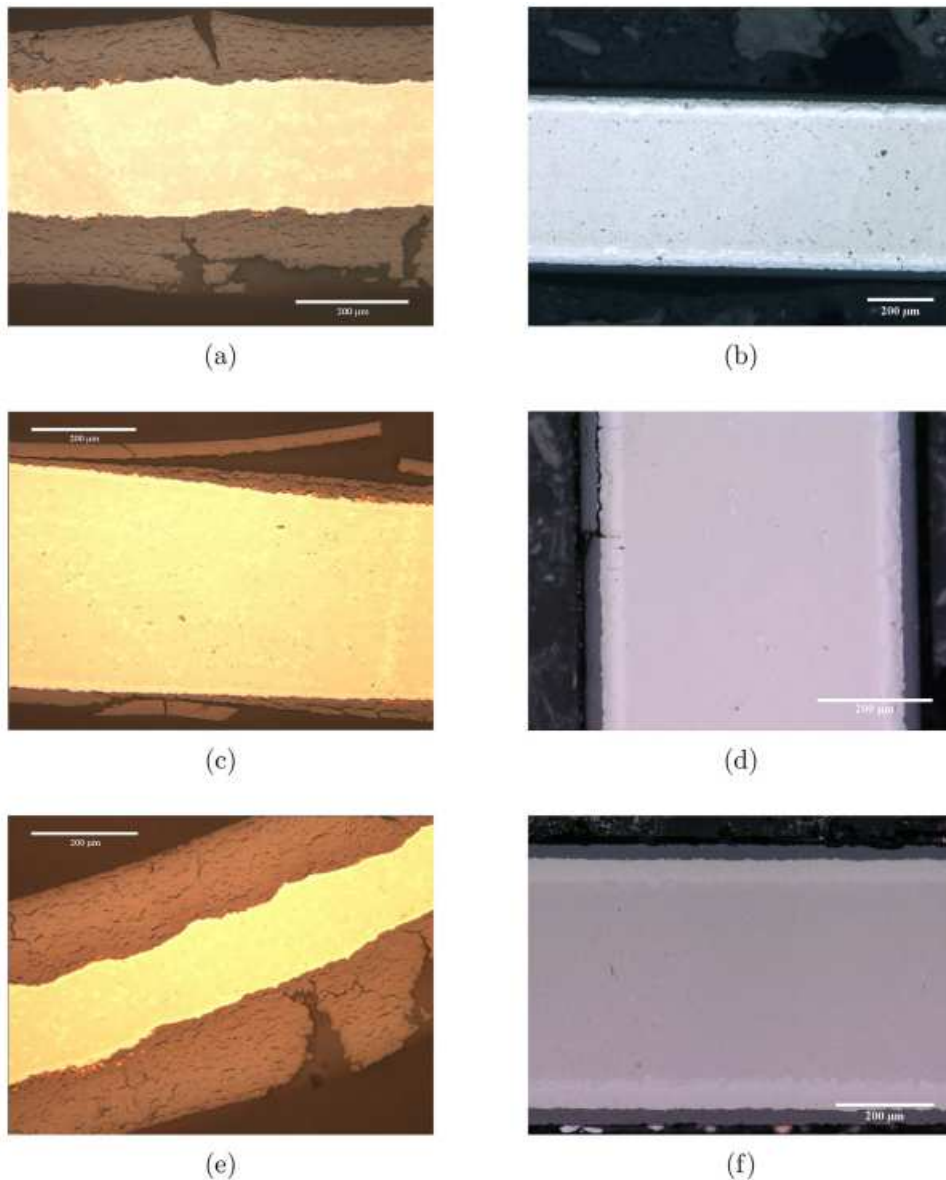


Fig. 6. Optical images of pre-oxidized Zy-4 plate samples after 850°C oxidation during 255 min (15300 s) (a) in 80 hPa O₂-320 hPa N₂, ECR_{HT}=35%; (b) in 80 hPa O₂, ECR_{HT}=4%; (c) in 320 hPa N₂-50 hPa H₂O, ECR_{HT}=15%; (d) in 50 hPa H₂O, ECR_{HT}=4%; (e) in 80 hPa O₂-320 hPa N₂-50 hPa H₂O, ECR_{HT}=37%; (f) in 80 hPa O₂-50 hPa H₂O, ECR_{HT}=5%. ECR_{HT} is the equivalent cladding reacted at high temperature as defined in paragraph 3.3.1.

The higher kinetic rates measured by thermogravimetric analysis when nitrogen is present in the gas phase is evidenced on the images. For a same exposure duration, the HT oxide scale is much thicker when nitrogen is added to the gas phase. The morphology of the pre-oxidized samples further annealed at high temperature in nitrogen-free atmospheres are quite similar. In particular, the pre-oxide scale is still adherent to the metal for almost the entire sample surface. An optical image of the samples edges is displayed in Fig. 8a and shows that HT oxide is present under the pre-oxide layer. However, even in these regions, no spalling of the oxide scales is evidenced. Some cracks may be detected in some places without apparent visual effects on oxidation kinetics. The morphology of the pre-oxidized samples further annealed at high temperature in nitrogen-containing atmospheres is completely different. In particular, the HT oxide formed under the LT pre-oxide is highly porous. Moreover, gold-colored particles are clearly detected close to the metal/oxide interface (Fig. 6a, 6c, 6e).

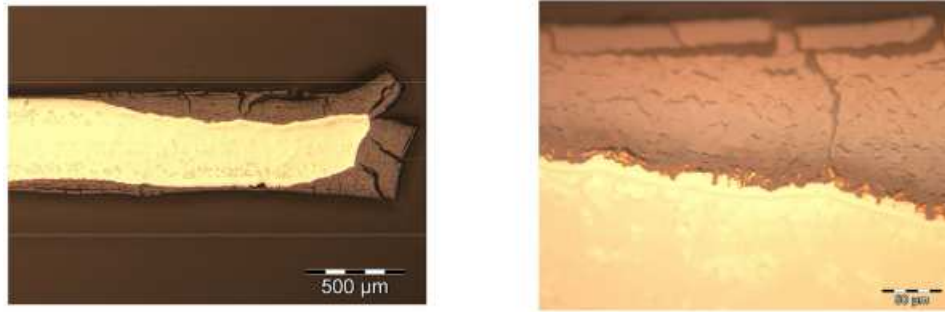


Fig. 7. Optical images at two different magnifications of a as-received Zy-4 plate sample after 850°C oxidation during 255 min (15300 s) in 80 hPa O₂-320 hPa N₂-50 hPa H₂O.



(a)



(b)

Fig. 8. Optical images of pre-oxidized Zy-4 plate samples after 850°C oxidation (a) during 255 min (15300 s) in 80 hPa O₂-50 hPa H₂O (b) during 26 min (1560 s) in 80 hPa O₂-320 hPa N₂-50 hPa H₂O.

Their nature was determined by Raman spectroscopy [10] and it was found that these are zirconium nitride particles. In fact, this HT oxide seems rather similar to that which is observed after the kinetic transition for bare Zy-4 material after similar oxidizing conditions (see Fig. 7). More importantly, the formation of this HT oxide in nitrogen-containing atmospheres induces an important spalling of the pre-oxide. This spalling is more or less pronounced, depending in particular on the oxidation duration. Scale cracking is now obvious. Here, it may be anticipated that such a spalling is not observed for nitrogen-free atmospheres, simply because the progress of the reaction is much slower. As already discussed [8,11,18], the presence of these zirconium nitride particles and their subsequent re-oxidation certainly play a role in the kinetic acceleration, as they do for bare Zy-4.

3.3. Determination of steam contribution to the oxidation process

3.3.1. Use of hydrogen released in the gas phase and incorporated in the metal

The analysis of the hydrogen concentration in the gas phase and incorporated in the alloy may be a means to determine if steam contributes to the oxidation process. Hydrogen release during the oxidation tests was monitored with a mass spectrometer. As a typical example, Fig. 9 compares the

mass gain rate and the hydrogen released in the gas phase versus time, for a test performed in a steam-nitrogen atmosphere, at 850°C, with a pre-oxidized plate. As the spectrometer was not carefully calibrated, the hydrogen signal, corrected from the water background, has been scaled arbitrarily. As can be seen in Fig. 9, there is a good correlation between the mass gain rate and the hydrogen released flow rate. When oxidation tests were performed in oxygen-steam-nitrogen atmospheres, at 850°C, with a pre-oxidized plate, hydrogen was not detected. One may conclude that the water molecule didn't contribute to the oxide formation. However, significant amount of hydrogen were incorporated in the metallic substrate during these tests (see Table 3). Additional blank tests, without Zy-4 samples, have been conducted at the same furnace temperature, using mixed atmospheres (hydrogen - oxygen - nitrogen). In such conditions (see Fig. 10), hydrogen was detected at the thermobalance outlet, but only in the first stage of the experiment. When isothermal conditions were reached, no more hydrogen was detected at the thermobalance outlet, meaning that hydrogen and oxygen have recombined in the gas phase to form water. For all the examined cases, the recombination between oxygen and hydrogen has led to a complete consumption of the hydrogen. This shows that the hydrogen release in the gas phase cannot be used to track the participation of the water molecule to the oxidation process in mixed atmospheres containing simultaneously oxygen and steam. Furthermore, at least in our experimental conditions, the absence of hydrogen in the gas phase is in no way a proof of an exclusive O₂ contribution. Conversely, the hydrogen uptake in the metal is an indisputable indicator of the participation of steam to the oxidation process.

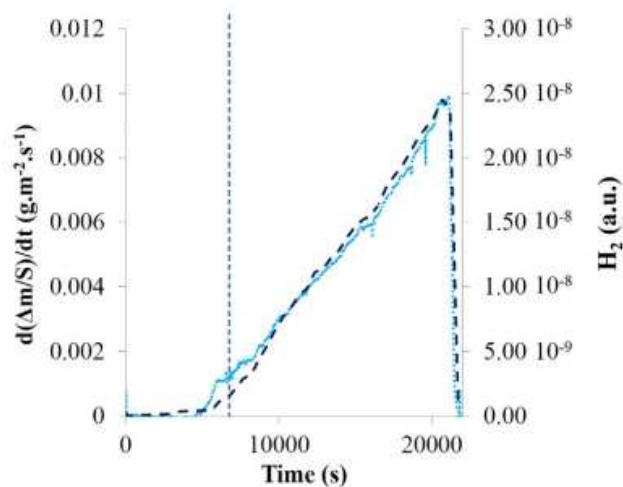


Fig. 9. Mass gain rate (dark blue) and hydrogen release (light blue) as a function of time during oxidation at 850°C in 50 hPa H₂O-320 hPa N₂ of a pre-oxidized Zy-4 plate sample.

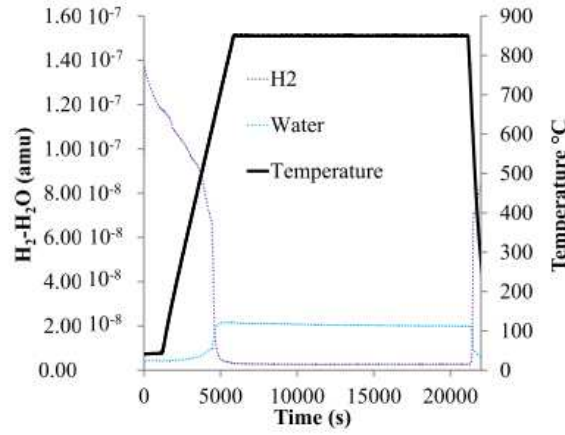


Fig. 10. Measurements by MS of hydrogen and steam as a function of time at 850°C in H₂-O₂-N₂.

Partial pressure (hPa)			ECR _{HT}	[H] _{HT}	Δ[H]
O ₂	N ₂	H ₂ O	(%)	(ppm)	(ppm)
0	0	50	4	649	342 ± 39
0	320	50	15	705	318 ± 65
80	320	0	35	487	37 ± 50
80	320	30	39	1016	341 ± 63
80	320	50	37	1201	475 ± 72
80	320	80	39	1568	672 ± 105
80	0	50	5	461	160 ± 27

Table 3. Hydrogen content in the metal for a pre-oxidized sample oxidized at HT.

Knowing the hydrogen content before and after the high temperature oxidation step, one can evaluate Δ[H] the hydrogen uptake during the high temperature reaction according to:

$$\Delta[H] = (1 - ECR_{HT}) \times [H]_{HT} - [H]_{PO} \quad (1)$$

where ECR_{HT} is the equivalent cladding reacted at high temperature, [H]_{HT} the hydrogen content in the metal after HT oxidation and [H]_{PO} the hydrogen content in the metal after the pre-oxidation step. With $m_{Zr,PO}$ the mass of Zr in the pre-oxidized sample, $m_{Zr,HT}$ the mass of Zr after the HT oxidation, $m_{H,PO}$ the mass of hydrogen in the pre-oxidized sample and $m_{H,HT}$ the mass of hydrogen after the HT oxidation, we have the following relations:

$$[H]_{PO} = \frac{m_{H,PO}}{m_{Zr,PO}} \quad (2)$$

$$[H]_{HT} = \frac{m_{H,HT}}{m_{Zr,HT}} \quad (3)$$

$$ECR_{HT} = 1 - \frac{m_{Zr,HT}}{m_{Zr,PO}} \quad (4)$$

Here, the ECR_{HT} was evaluated from the oxygen mass gain during the HT oxidation (Δ m_{HT}), assuming that the mass gain is due to the conversion of the Zr into stoichiometric ZrO₂:

$$ECR_{HT} = \Delta m_{HT} \times \frac{(M_{Zr}/2M_O)}{m_{Zr,PO}} \quad (5)$$

with M_{Zr} the molar mass of Zr and M_O the molar mass of oxygen.

$\Delta[H]$ calculated by Equation 1 is a net hydrogen balance, including incorporation and possible desorption of the hydrogen already present during the pre-oxidation phase. Values given in Table 3 show that incorporation always dominates, as negative values were never observed. For the test in dry air, $\Delta[H]$ was close to zero, showing that no desorption occurred. The hydrogen uptake strongly varies with the composition of the atmosphere, as well as with the ECR_{HT} parameter. For comparable ECR_{HT} , there is a strong correlation of the hydrogen pick-up with the steam partial pressure in the gas phase, as represented on Fig. 11: the higher the steam partial pressure, the higher the hydrogen up-take. This is a strong indication that, even if H_2 is not detected by mass spectrometry in the gas phase, steam participates to the overall corrosion process with a contribution depending on its partial pressure. The objective of the next section is to quantify this effect. Strong hydrogen incorporation during high temperature oxidation of Zircaloy-4 was already observed in nitrogen-steam [20] as well as in air-steam mixtures [24]. A mechanism, involving hydrogen trapping and concentrating in the porosities of the oxide close to the reacting surface, was proposed to explain hydrogen incorporation during steam oxidation of zirconium alloy at high temperature [25]. Owing to the strongly porous oxide formed in nitrogen containing atmospheres, the same mechanism was invoked in [24,26] and can also explain the present results.

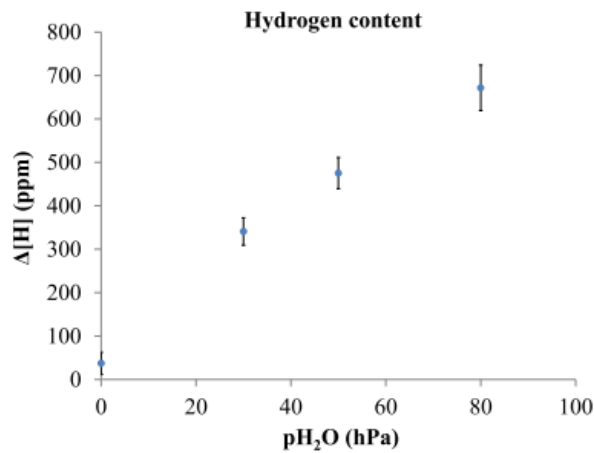


Fig. 11. Hydrogen pick-up in the metal during HT oxidation under air-steam (80 hPa O_2 -320 hPa N_2 -x hPa H_2O) of a pre-oxidized sample. ECR_{HT} is $\approx 37\%$.

3.3.2. ^{18}O isotopic labelling

A convenient means to try to answer this question is to use an isotopic tracer, here ^{18}O . For such a purpose, mixed $^{18}O_2$ - H_2 - ^{16}O - N_2 atmospheres were used for preliminary tests conducted on both bare and pre-oxidized Zy-4 samples. For experimental reasons (^{18}O availability), low ^{18}O and water partial pressures had to be used. Here, the $^{18}O/^{16}O$ ratio has been adjusted to 3.2, corresponding to a $^{18}O/O$ ratio of 76%. In fact, the monitoring of the gas phase by mass spectrometry showed a slight isotopic exchange, as well as a residual contamination by $^{16}O_2$. As a result, the actual $^{18}O_2/(^{16}O_2 + ^{18}O_2)$ ratios was 96% for the test with bare Zy-4 and 87% for the test with pre-oxidized sample. Moreover, a large amount of $H_2^{18}O$ was detected, since the measured $H_2^{16}O/(H_2^{16}O + H_2^{18}O)$ ratio was around 50%. $H_2^{18}O$ was probably formed by the following reaction in the gas phase: $^{18}O_2 + H_2 \rightarrow H_2^{18}O$. Its concentration was nearly constant during the oxidation tests. In spite of these uncertainties on the gas phase composition, some trends can be extracted from these preliminary isotopic labelling measurements.

The tests conducted on bare Zy-4 samples are probably the simplest to interpret, because, for rather low exposition times, they minimize the effects of isotopic exchange within the zirconia grains. Indeed, two-stage oxidation measurements made it possible to highlight two different oxygen diffusion paths, grains and grain boundaries [22]. They also strongly suggest a preferential diffusion path along the grain boundaries. Anyway, isotopic exchange within grains cannot be completely neglected. Two examples are first shown in Fig. 12. The optical images allow to identify two different regions: the dense oxide formed before the kinetic transition, and the porous oxide formed after the kinetic transition. ZrN grains are also evidenced as golden particles. Within the experimental accuracy, the corresponding ^{18}O concentration images first show that in the porous oxide, the measured content is in the 70-75% range, i.e. very close to the targeted $^{18}\text{O}/\text{O}$ ratio present in the gas phase (76%). This preliminary measurement allows to conclude with certainty that the contribution of O_2 and H_2O to the oxidation process corresponds to their respective concentration in the gas phase. On the other hand, in the protective, dense oxide layer, the one which is first formed at the Zy-4 surface, the oxide ^{18}O content is significantly lower. The two images show concentrations close to 55-60% in the lower part of this layer, with a slightly higher value close to the surface. Firstly, this is an indication that the dense pre-transition oxide is rather formed from steam than from oxygen. This is the only way to explain such a low ^{18}O content in the corrosion scale. Secondly, the slightly higher ^{18}O content close to the scale surface is an indication that some isotopic exchange between the scale and the gas phase occurred, all the more important that the sample exposition to the gas phase is high. This is not an unexpected result in that the surface of the layer is in contact with the gaseous phase, so tend to equilibrate with it. Thus, in this particular case, isotopic labelling makes it possible to confirm that the rate-limiting steps for the kinetics of formation of the oxide are different before and after the kinetic transition. Actually, it was demonstrated in previous publications that the kinetic mechanism is completely different between the pre and post-transition regimes for as-received Zy-4 or ZrNbO samples oxidized between 500 and 550°C in steam [27,28] and for as-received Zy-4 samples oxidized at 850°C in dry air [11]. In the post-transition regime, a significant influence of steam partial pressure (when Zy-4 or ZrNbO samples are oxidized in steam) or oxygen partial pressure (when Zy-4 samples are oxidized in dry air) has been found, contrarily to the kinetic behavior before the transition. These differences between the pre- and the post-transition from a kinetic point of view can explain that the respective reactivity of oxygen and steam are not the same before and after the transition. Note that because the oxygen and steam flow rates were very low for these tests (see Table 2), oxygen and steam starvation cannot be excluded, specifically for the test with the bare specimen, at the beginning of the dense oxide layer formation.

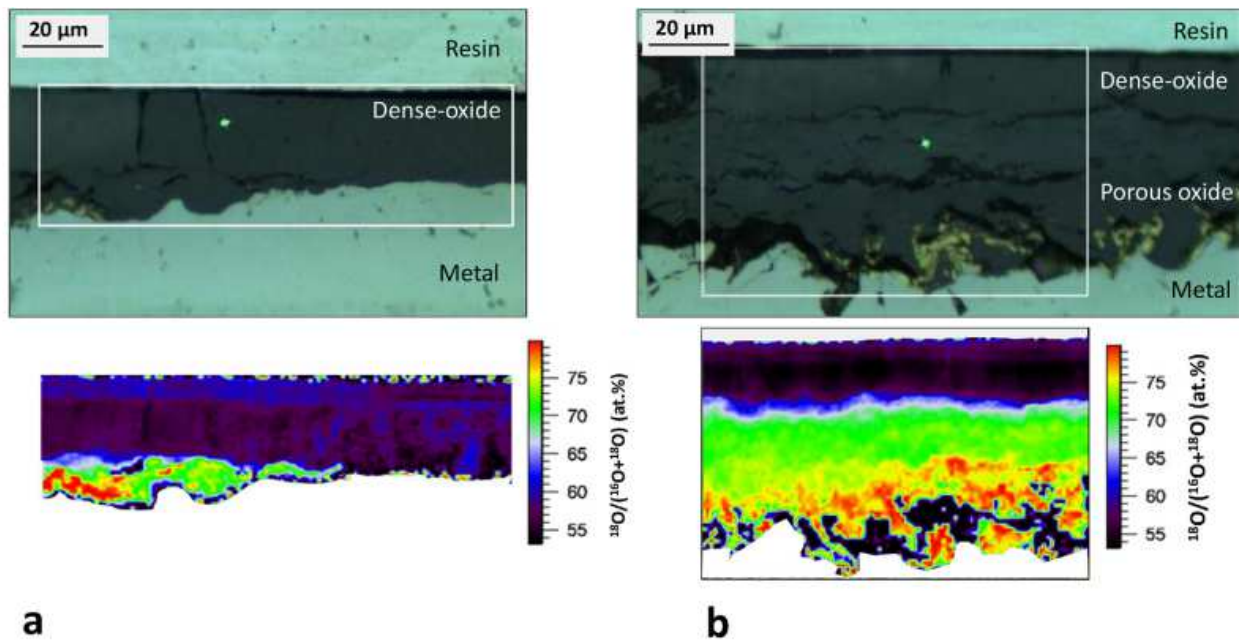


Fig. 12. As-received Zy-4 after 150 min exposure to $^{18}\text{O}_2+\text{H}_2^{16}\text{O}+\text{N}_2$ at 850°C with $^{18}\text{O}/(^{18}\text{O}+^{16}\text{O}) = 76\%$. Optical bright-field image and ^{18}O distribution map on two different zones (a) dense pre-transition oxide on the right-hand side of the pictures (porous post-transition oxide can be distinguished on the left-hand side of the pictures), (b) porous post-transition oxide.

The two images obtained during the analysis of a pre-oxidized sample and then subjected to the same atmosphere as the bare Zy-4 are shown in Fig. 13. The first one (Fig. 13a) was obtained in an area where the pre-oxide is still adherent and the HT oxide is not clearly detected. The image simply shows the progressive ingress of oxygen through the pre-oxide layer. The ^{18}O concentration map shows that ^{18}O has not penetrated throughout the scale, as no ^{18}O is found in the $\approx 20\ \mu\text{m}$ innermost oxide. The full width at half maximum (FWHM) map shows that, in region where ^{18}O is present, the width of the $475\ \text{cm}^{-1}$ line is much higher than the maximum width measured for standard powdered samples. The reason of this peak broadening is again a ^{18}O concentration gradient between the periphery and the core of the grains. Note that the ^{18}O distribution appears not to be homogeneous in the direction parallel to the surface, and that the thickness of the layer having high ^{18}O content varies from ≈ 5 to $\approx 10\ \mu\text{m}$. Non uniformity of the ^{18}O distribution map in Fig. 13a likely reveals non-uniformity of the oxygen diffusion through the pre-oxide scale. This was already observed in previous works [19]. Corrosion scales formed on the Zy-4 alloy are known to show a non-uniform microstructure in the direction parallel to the surface, with alternatively dense veins and more cracked regions. A possible influence of such non-uniformities on the oxygen diffusion has been discussed with more details in [20]. This map is consistent with the low weight gain during the HT exposure, and indicates that after 125 min at 850°C in the reacting atmosphere, some barrier effect of the pre-oxide scale is effective far from the sample edges. The second ^{18}O concentration image (Fig. 13b) was obtained close to a sample edge, where a thick layer of HT oxide has formed under the peeled-off pre-oxide scale. It shows a rather homogeneous ^{18}O content, again in the 70e75% range. The average concentration is similar to that estimated after the analysis of the bare Zy-4 sample oxidized at HT in the post-transition areas. Again, this ^{18}O content suggests that neither the O_2 nor the H_2O molecules are favoured in the oxidation process, meaning that their respective contribution corresponds to their concentration in the gas phase. Note also the high content of ^{18}O in the upper part of the layer, corresponding to the pre-oxide. This means that in this region, the isotopic

exchange is very strong, most probably due to the creation of cracks that allows a straightforward ingress of the reacting gas mixture within the pre-oxide.

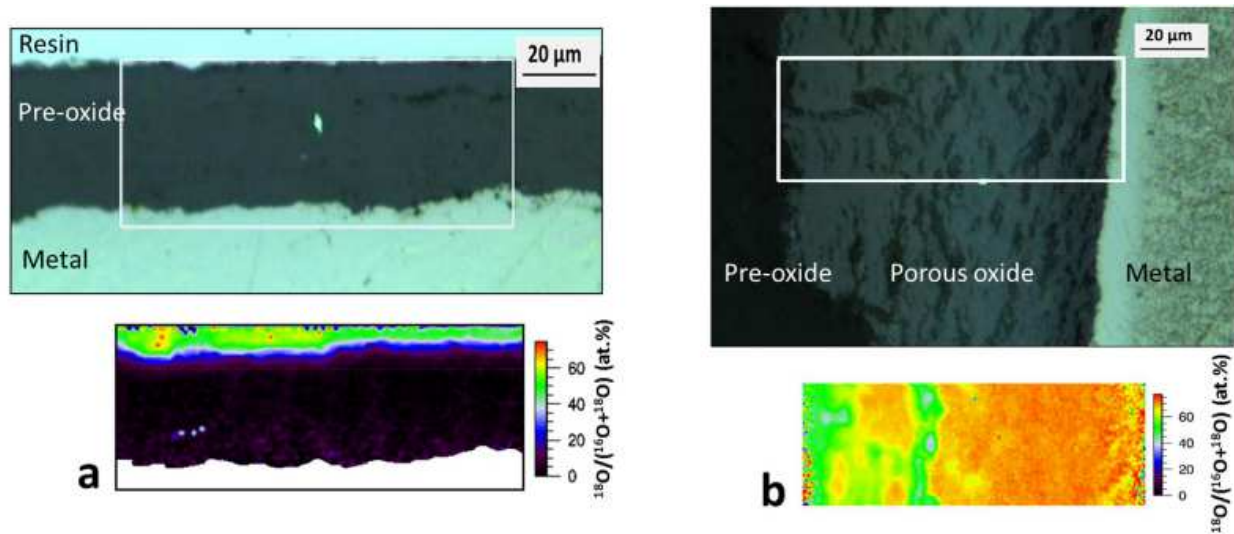


Fig. 13. Pre-oxidized Zy-4 plate after 125 min (7500 s) exposure to $^{18}\text{O}_2+\text{H}_2^{16}\text{O}+\text{N}_2$ at 850°C . Optical bright-field image and ^{18}O distribution map, (a) pre-oxidation layer, (b) porous HT oxide.

4. Discussion

Earlier studies have obviously shown the strong effect of air and especially of nitrogen on the degradation of Zr-based cladding. In this study, experimental results clearly show the same effect with Zy-4 plates pre-oxidized at low temperature, i.e. a fast oxidation when O_2 and/or H_2O is mixed with N_2 . Addition of N_2 to O_2 and/or H_2O increases the kinetic rate up to a factor of 10 (see Fig. 4). The effect of high temperature oxidation in air-steam of pre-oxidized samples is displayed on Fig. 14 where photographs of different samples exposed to nitrogen-containing atmospheres during increased time durations are displayed. Analysis of the thermogravimetric data obtained at 850°C reveals that, contrary to as-received Zy-4, the oxidation process can not be described by the formation of a protective oxide scale followed by a breakaway transition. After a short slight decrease, the mass gain rate becomes continuously increasing, but not at the same rate during the whole oxidation experiment. The kinetic curves obtained under air or air-steam can actually be decomposed into three parts (see Fig. 4c):

- Once the temperature plateau is reached, the mass gain rate increases regularly and moderately during the first ≈ 7000 s (first acceleration period),
- Afterwards, there is a slope change in the mass gain rate curve and oxidation continues at a higher rate during the next ≈ 4000 s (second acceleration period),
- Then, the mass gain rate increases very smoothly (third acceleration period).

A description of these three periods is given hereafter.

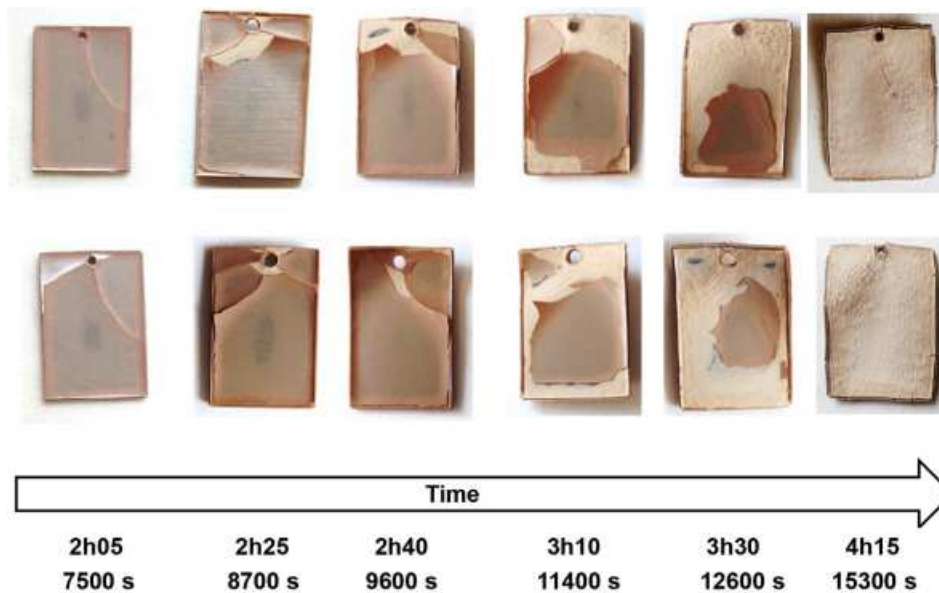


Fig. 14. Time effect on the loss of protectiveness of the pre-oxide scale. For each time duration, the two photographs correspond to the two sides of the sample.

4.1. First acceleration period

When isothermal conditions are reached, the kinetic rate, in the $0.001\text{-}0.0015\text{ g m}^{-2}\text{ s}^{-1}$ range, does not depend on the presence of nitrogen in the gas phase (the initial kinetic rate is the same for both curves in Fig. 4c). Then, the mass gain rate increases regularly if nitrogen is present, whereas it remains nearly constant if it is not. This increase of the oxidation rate is an indication that shortly after the beginning of the isothermal conditions, the pre-oxide scale loses its protectiveness. Examination of sample metallographies close to edges of the sample shows that the HT oxide is visible below the cracks. This is noticeable with nitrogen-free (see Fig. 8a) or nitrogen-containing (see Fig. 3b) atmospheres. The morphology of the HT oxide layer formed in nitrogen-containing atmospheres is very similar to the oxide formed on bare Zy-4 after the kinetic transition: the HT scale is porous and exhibits cracks parallel to the surface sample and zirconium nitride precipitates are noticeable near to the metal/oxide interface [7-10]. The degradation process could consequently be the same as the one proposed for bare Zy-4 in [7,8], i.e. the formation of zirconium nitride near the oxide/metal interface which acts as a “catalyst”. However, whereas for bare Zy-4, we observe the random surface nucleation of attacked regions, forming nodules of porous oxide that progressively extend laterally and inwards, for pre-oxidized plate samples, the HT oxide first grows below the cracks located at the sample edges and progresses laterally from the edges to the center of the sample. When nitrogen is present in the atmosphere, we observe that the growth of the HT oxide on the edges of the sample causes the progressive detachment of the pre-oxide layer. The fraction of the surface affected by spalling of the pre-oxide layer and the associated fast HT oxidation progresses laterally in the sample, as shown in Fig. 3b. This effect is also noticeable on Fig. 14. Optical microscopy and macrographs of the samples have been used to measure the progressive extent of the zone with non-protective scale during this first phase. For samples oxidized under air or air-steam mixtures, it is in the $8\text{-}9\text{ }\mu\text{m min}^{-1}$ range and very reproducible from one sample to another one. At the end of the first acceleration period, the mass gain rate is $\approx 0.006\text{ g m}^{-2}\text{ s}^{-1}$ for samples oxidized under air-steam (Fig. 4c). To suppress this edge effect, different solutions were considered in [20]. The results obtained with pre-oxidized beads revealed a very efficient protective effect of the

pre-oxide scale regarding air attack at high temperature. Nevertheless, as any defect of the pre-oxide scale may be an initiator of its failure, it is important to study how the HT oxidation progresses, once it has started.

4.2. Second acceleration period

The second period is characterized by a faster increase of the mass gain rate, but it was not possible to retrieve it directly from micrographs. The kinetic curves show (see Fig. 15) that the acceleration during the second phase depends on the pre-oxide thickness, at least in the 26.6-32.7 μm investigated range. The acceleration is slower for the thicker pre-oxide scales. The strong kinetic acceleration and the spalling of the pre-oxide layer is characteristic of the oxidation under nitrogen-containing atmospheres since it was not observed for HT oxidation under nitrogen-free atmospheres (or to a much smaller extent). The detachment of the pre-oxide layer is probably due to the high stresses induced by the different reactions namely the oxidation of the $\alpha\text{-ZrO}$ phase into zirconia (volume increase with a Pilling and Bedworth ratio $\text{PBR}_{\text{ZrO}_2/\text{Zr}}$ of 1.56) and the oxidation of ZrN precipitates (volume increase with a molar volume ratio ZrO_2/ZrN of 1.47). The fast growth of the HT oxide under nitrogen-containing atmospheres, which initiates on the edges and then propagates to the whole sample, is due to the porosity of the HT cracked oxide layer and to the spalling of the pre-oxide layer which both enables the reacting gases to have a direct access to the metal. Some tests in air-steam mixture were interrupted at the end of the second acceleration period. It is observed that the HT oxide grown under the pre-oxide has spread to the whole specimen's surface.

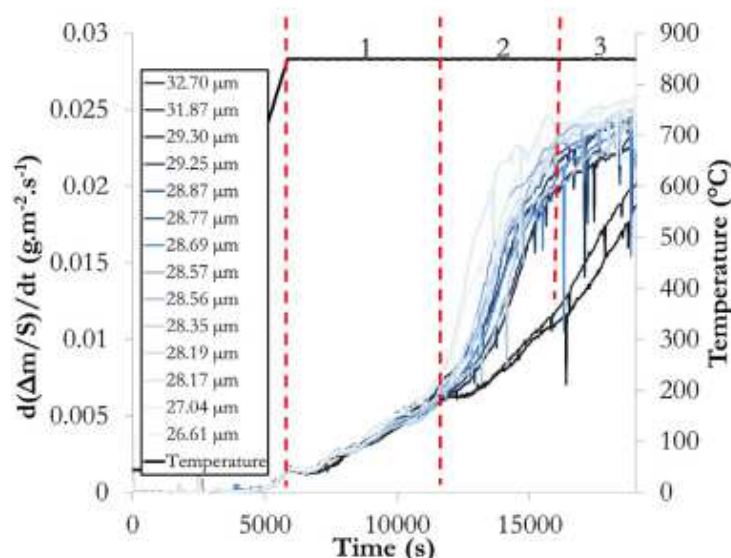


Fig. 15. Mass gain rate as a function of time in 80 hPa O_2 -320 hPa N_2 -50 hPa H_2O , at 850°C for samples having various pre-oxide thicknesses, as indicated on the graph.

4.3. Third acceleration period

During the third acceleration period, the mass gain rate increase is much slower. This slow increase can be attributed to the creep of the sample, which is known to be very significant when nitrogen is present in the reactive gas [4]. This has been confirmed thanks to dilatometry measurements, that make possible to follow the dimensional variations of a sample as a function of time. Dilatometry measurements were performed in isothermal conditions using a SETARAM TMA dilatometer with as-

received Zircaloy-4 tubes of 0.57 mm in thickness, 0.93 mm in diameter and 2-5 mm in height with two exactly parallel faces. The results are shown in Fig. 16, and the measured creep rate calculated from the slope of the dimension change curve is $1.65 \cdot 10^{-5} \text{ s}^{-1}$. It allows to explain the velocity of the mass gain rate increase during the third phase, which is approximately $2 \cdot 10^{-5} \text{ s}^{-1}$ (computed as the difference between the mass gain rate at the end and the beginning of phase 3 divided by the mass gain rate at the beginning of phase 3 and time duration of phase 3).

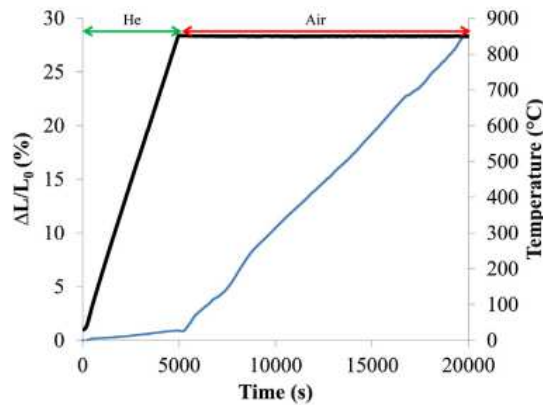


Fig. 16. Samples expansion as a function of time in air at 850°C for as-received Zy-4 tube samples.

Finally, the kinetic curves obtained with pre-oxidized plate samples have been compared to thermogravimetric data measured in dry air at 850°C on pre-oxidized Zircaloy-4 tube segments (9.5 mm outer diameter, 0.570 mm wall thickness, 20 mm length, pre-oxide scale of about 30 μm thickness) [19]. For these experiments, the partial pressures of N_2 and O_2 were 800 and 200 hPa respectively. The mass gain rates, shown in Fig. 17, are quite similar for both geometries. We can notice that the increase of the mass gain rate during the first phase (the first 7000 s) is greater for the plate sample for which the ratio of the sample edges length to the surface area is higher ($\approx 0.33 \text{ mm}^{-1}$ for the plate sample, 0.1 mm^{-1} for the tube sample). The progressive spalling during this phase, which is responsible for the kinetic acceleration for plate samples, seems to be less pronounced for tube samples. Both samples exhibit a fast kinetic rate increase during the second phase to reach a mass gain rate which is roughly the same in both cases. It means that the complete spalling of the pre-oxide scale occurs for both geometries. In the third phase, the slow mass gain rate increase is slightly greater for the tube sample.

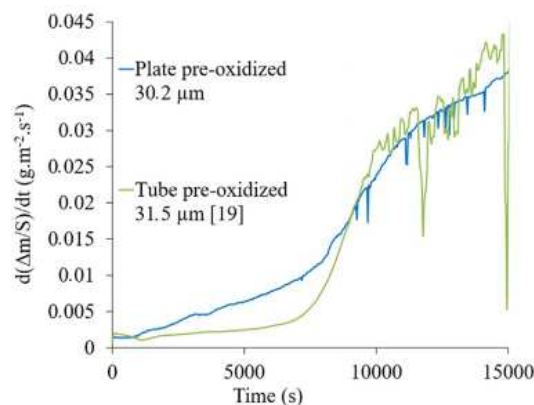


Fig. 17. Weight gain rate recorded during isothermal oxidation in 800 hPa N_2 -200 hPa O_2 at 850°C of pre-oxidized Zircaloy-4 specimens with plate or tube [19] geometry.

5. Conclusion

In order to study the influence of a pre-oxide layer on the behavior of Zircaloy-4 exposed at 850°C to atmospheres representative of SFPs accidental conditions, corrosion tests in oxygen-steam-nitrogen mixed atmospheres have been performed. Oxidation in dry air, in wet air or in a steam-nitrogen atmosphere leads to fast oxidation and to strong degradation of the cladding material. Experimental characterizations have evidenced that the initial increase of the mass gain rate, which is moderate, is linked to the progressive spalling of the pre-oxide scale that initiates on the edges of the samples. The following strong increase of the mass gain rate is due to the spalling of the remaining pre-oxide layer, and the final slow increase can be explained by the creep of the sample. Moreover, the morphology of the HT oxide layer is very similar to that observed on bare Zy-4 after the kinetic transition. We can consequently conclude from these observations that cracks in the pre-oxide layer play a crucial role in the loss of protectiveness of the scale. Nitrogen-“catalyzed” fast oxidation initiates there and then propagates laterally to the whole specimen's surface. The propagation is associated to delamination and breakdown of the scales. The mechanism proposed for air oxidation of bare Zy-4, namely nitride oxidation, α -Zr(O) nitridation and oxidation is also applicable to pre-oxidized Zy-4. The main difference between bare and pre-oxidized samples lies in the dimensions of the zone where the rate-determining step takes place. For pre-oxidized sample, it is linked to the progressive detachment of the pre-oxide layer. As the spalling strongly depends on the stresses and consequently on the geometry, we note some differences between samples with different geometry (plate and sample). Nevertheless, the complete spalling finally occur on both geometries leading to the exposure of the whole surface sample to the reacting gases.

The different experimental techniques used in this study have also put in evidence that O₂ and H₂O both contribute to the oxidation process, despite the very moderate increase of the kinetic rate when steam is added to air (from 30 to 80 hPa). The first evidence was provided by hydrogen pick-up measurements by the fusion technique. They show that the H₂ content in a sample after HT oxidation is correlated to the steam fraction in the atmosphere during the HT oxidation, which is an indication of steam contribution to the oxidation process. The second evidence was provided by images obtained by Raman spectroscopy after having exposed a pre-oxidized sample to a ¹⁸O/H₂¹⁶O mixture. With the gas composition used for the ¹⁸O measurements, the ¹⁸O/¹⁶O ratio in the porous HT oxide is the same as the ¹⁸O/¹⁶O ratio in the gas phase. These measurements also demonstrate that Raman spectroscopy is a powerful technique to image the localisation of ¹⁸O after isotopic labelling experiments. Thanks to this experimental study, a number of kinetic data have been acquired and different techniques have been used to characterize the samples. This study continues in order to propose a kinetic modelling of the oxidation in air-steam of pre-oxidized Zy-4. From a safety point of view, it can be inferred from these results that in case of a SFP deflooding accident, the corrosion scale grown on the cladding tubes during normal operation will have some protective effect regarding further oxidation by air and steam. However, local defects such as scratches or oxide spalling sometimes encountered will be weakness spots where the nitrogen-“catalyzed” fast oxidation will initiate and progressively propagate laterally. More importantly, ballooning will occur due to the internal pressure of the fuel rods, and failure of the corrosion scale is here unavoidable.

Acknowledgment

This work has been performed in the frame of the DENOPI project, funded by the French government as part of the Investment for the Future Program, reference ANR-11-RSNR-0006. We warmly thank the whole DENOPI consortium for fruitful comments and discussions.

References

- [1] Status Report on Spent Fuel Pools under Loss-Of-Cooling and Loss-Of-Coolant Accident Conditions, Report NEA/CSNI/R vol. 2, OECD, 2015, 2015.
- [2] I. Shepherd, Oxidation Phenomena in Severe Accidents (OPSA), Report INV-OPSA(99)-P008, EUR 19528 EN, 2000.
- [3] E.T. Hayes, A.H. Roberson, Some effects of heating zirconium in air, oxygen and nitrogen, *J. Electrochem. Soc.* 96 (1949) 142-151.
- [4] E.B. Evans, N. Tsangarakis, H.B. Probst, N.J. Garibotti, Critical role of nitrogen during high temperature scaling of zirconium, in: *Proceedings of the Conference on Metallurgical Society of AIIME, Symposium on High Temperature Gas Metal Reactions in Mixed Environments*, 1972.
- [5] S. Leistikow, H.V. Berg, Investigation under nuclear safety aspects of zircaloy-4 oxidation kinetics at high temperature in air, in: *Proceedings of the 2nd Workshop of German and Polish Research on High Temperature Corrosion of Metals*, 1987.
- [6] K. Natesan, W.K. Soppet, Air Oxidation Kinetics for Zr-Based Alloys, Report 03/32, NUREG/CR-6846, Argonne National Laboratory, 2004.
- [7] C. Duriez, T. Dupont, B. Schmets, F. Enoch, Zircaloy-4 and M5 high temperature oxidation and nitriding in air, *J. Nucl. Mater.* 380 (2008) 30-45.
- [8] M. Steinbrück, Prototypical experiments related to air oxidation of Zircaloy-4 at high temperatures, *J. Nucl. Mater.* 392 (2009) 531-544.
- [9] M. Lasserre, V. Peres, M. Pijolat, O. Coindreau, C. Duriez, J.P. Mardon, Qualitative analysis of Zircaloy-4 cladding air degradation in O₂-N₂ mixtures at high temperature, *Mater. Corros.* 65 (2014) 250-259.
- [10] I. Idarraga, M. Mermoux, C. Duriez, A. Crisci, J.P. Mardon, Raman investigation of pre- and post-breakaway oxide scales formed on Zircaloy-4 and M5 in air at high temperature, *J. Nucl. Mater.* 421 (2012) 160-171.
- [11] M. Lasserre, V. Peres, M. Pijolat, O. Coindreau, C. Duriez, J.P. Mardon, Modelling of Zircaloy-4 accelerated degradation kinetics in nitrogen-oxygen mixtures at 850°C, *J. Nucl. Mater.* 462 (2015) 221-229.
- [12] M. Negyesi, M. Amaya, Oxidation behavior of zry-4 in steam-air mixtures at high temperature, in: *Proceedings of 2016 Water Reactor Fuel Performance Meeting (WRFPM)*, 2016.
- [13] T. Kawasaki, S. Furuta, M. Suzuki, Oxidation of zircaloy-4 under high temperature steam Atmosphere and its effect on ductility of cladding, *J. Nucl. Sci. Technol.* 15 (1978) 589-596.
- [14] S. Guilbert, C. Duriez, C. Grandjean, Influence of a pre-oxide layer on oxygen diffusion and on post-quench mechanical properties of zircaloy-4 after steam oxidation at 900°C, in: *Proceedings of 2010 Water Reactor Fuel Performance Meeting (WRFPM)*, 2010.
- [15] S. Guilbert, P. Lacote, G. Montigny, C. Duriez, J. Desquines, C. Grandjean, Effect of pre-oxide on zircaloy-4 high-temperature steam oxidation and post-quench mechanical properties, in: *Proceedings of Zirconium in the Nuclear Industry, 17th International Symposium*, 2014.

- [16] M. Le Saux, J.-C. Brachet, V. Vandenberghe, Influence of pre-transient oxide on LOCA high temperature steam oxidation and post-quench mechanical properties of zircaloy-4 and M5 cladding, in: Proceedings of 2011 Water Reactor Fuel Performance Meeting (WRFPM), 2011.
- [17] B. Mazeres, C. Desgranges, C. Toffolon-Masclat, D. Monceau, Experimental study and numerical simulation of high temperature (1100-1250°C) oxidation of prior-oxidized zirconium alloy, *Corros. Sci.* 103 (2016) 10-19.
- [18] C. Duriez, D. Drouan, G. Pouzadoux, Reaction in air and in nitrogen of pre-oxidized Zircaloy-4 and M5™ claddings, *J. Nucl. Mater.* 441 (2013) 84-95.
- [19] A. Kasperski, C. Duriez, M. Mermoux, Combined Raman imaging and ¹⁸O tracer analysis for the study of Zircaloy-4 high temperature oxidation in spent fuel pool accident, in: Proceedings of Zirconium in the Nuclear Industry, 18th International Symposium, 2016.
- [20] C. Duriez, O. Coindreau, M. Gestin, A. Kasperski, V. Peres, M. Pijolat, H. Buscail, C. Issartel, R. Rolland, M. Mermoux, Zircaloy-4 high temperature oxidation in atmospheres representative of SFP-LOCA: investigation of the influence of a low temperature pre-oxidation scale, *J. Nucl. Mater.* 513 (2019) 152-174.
- [21] C. Raepsaet, P. Bossis, D. Hamon, J.L. Bechade, J.C. Brachet, Quantification and local distribution of hydrogen within Zircaloy-4 PWR nuclear fuel cladding tubes at the nuclear microprobe of the Pierre Süe Laboratory from m-ERDA, *Nucl. Instrum. Methods Phys. Res. Sect. B Beam Interact. Mater. Atoms* 266 (10) (2008) 2424-2428.
- [22] M. Guerain, M. Mermoux, C. Duriez, The use of micro-Raman imaging to measure ¹⁸O tracer distribution in thermally grown zirconia scales, *Corros. Sci.* 98 (2015) 140-149.
- [23] A. Kasperski, M. Guerain, M. Mermoux, F. Jomard, High-temperature oxidation of Zircaloy-4 in air studied with labeled oxygen and Raman imaging, *Oxid. Metals* 87 (3) (2017) 501-513.
- [24] M. Negyesi, M. Amaya, The influence of the air fraction in steam on the growth of the columnar oxide and the adjacent α -Zr(o) layer on Zry-4 fuel cladding at 1273 and 1473 K, *Ann. Nucl. Energy* 114 (3) (2018) 52-65.
- [25] M. Grosse, E. Lehmann, M. Steinbrück, G. Kühne, J. Stuckert, Influence of oxide layer morphology on hydrogen concentration in tin and niobium containing zirconium alloys after high temperature steam oxidation, *J. Nucl. Mater.* 385 (2) (2009) 339e345.
- [26] M. Steinbrück, F.O. da Silva, M. Grosse, Oxidation of Zircaloy-4 in steam-nitrogen mixtures at 600-1200°C, *J. Nucl. Mater.* 490 (2017) 226e237.
- [27] M. Tupin, M. Pijolat, F. Valdivieso, M. Soustelle, A. Frichet, P. Barberis, Differences in reactivity of oxide growth during the oxidation of Zircaloy-4 in water vapour before and after the kinetic transition, *J. Nucl. Mater.* 317 (2003) 130e144.
- [28] M. Tupin, M. Pijolat, F. Valdivieso, M. Soustelle, Oxidation kinetics of ZrNbO in steam: differences between the pre- and post-transition stages, *J. Nucl. Mater.* 342 (2005) 108e118.